Total neutron cross section for ^{151}Sm and nuclear systematics of the Sm isotopes

G. J. Kirouac and H. M. Eiland
Knolls Atomic Power Laboratory, Schenectady, New York*
(Received 5 September 1974)

The energy dependent total neutron cross section of ^{151}Sm, a fission product poison, has been measured from thermal neutron energies up to about 2.3 keV. The results obtained for the thermal (0.0253 eV) cross section, resonance integral, s-wave level spacing, and strength function were: 15 200 ± 300 b, 3520 ± 160 b, 1.72 ± 0.07 eV, and $S_0 = 3.65 \pm 0.48 \times 10^{-4}$, respectively. The neutron widths for 120 resonances up to 300 eV were obtained by conventional analytic methods and the radiation widths were also obtained for 13 low energy resonances. The strength function was derived from resolved neutron resonances and from the average keV cross section. In addition, the Dyson-Mehta Δ_3 statistic was calculated from the level sequences of Sm isotopes and compared with the prediction of the statistical orthogonal ensemble. The level densities of six Sm isotopes and seven Nd isotopes were used to compute the Fermi level density parameter a, and these results are discussed in light of the nuclear structure. Finally, the systematic behavior of s-wave strength functions in the $142 \leq A \leq 158$ mass region is examined.

[NUCLEAR REACTIONS ^{151}Sm(n,n), (n,γ), $E = 0$–2.5 keV; measured $\sigma_t(E)$; deduced E_0, $g\Gamma_n$, Γ_γ, S_0, $\langle D_0 \rangle$; O.E. theory test; studied systematics S_0, $\langle D_0 \rangle$ for $142 \leq A \leq 158$.]

INTRODUCTION

^{151}Sm is a fission product poison produced in thermal nuclear reactors.[1-3] It has an evaluated ^{235}U fission yield of 0.42%[4] and a thermal cross section[3] of about 15 000 b. Because it has a half-life of 93 yr, it accumulates in the core until it undergoes neutron capture.

The only energy dependent measurement of the ^{151}Sm cross section was made by Pattenden[3] using a sample containing less than 4 at.% ^{151}Sm. Neutron resonance widths, but no radiation widths, were reported up to 13 eV. The shape of the low energy cross section was observed to be strongly non-$1/v$.

In addition to the importance of ^{151}Sm as a fission product poison, it and the other Sm isotopes are interesting from a nuclear structure viewpoint. The isotopes of Sm occupy the mass region near the first peak in the split 4-s giant resonance. They may also be thought of as transition nuclei between nearly spherical vibrators (^{144}Sm) and permanently deformed rotators (^{154}Sm). In an oversimplified shell model picture, the ground state of the Sm isotopes has two proton holes in the $2d_{5/2}$ shell and a varying number of neutrons in the $1h_{9/2}$ or $2f_{7/2}$ shells. Since extensive cross section data, including resonance parameters, level spacings, and strength functions, are already available for five other Sm isotopes, it is of interest to examine the systematic behavior of these nuclear properties.

In this work a brief account is given of a standard time-of-flight measurement of the ^{151}Sm total neutron cross section from thermal energies to the low keV range. The resonances are analyzed by both shape and area methods to provide neutron widths Γ_n and radiation widths Γ_γ. Parameters for 120 levels up to about 300 eV are reported and the s-wave strength function S_0 and level spacing are determined. The strength function derived from the resolved resonances is also compared with that obtained from the keV average cross section. Three different averaging intervals are used to illustrate structure in the neutron cross section from 100–2200 eV. The distribution of the level spacings for Sm isotopes is also tested against the Dyson-Mehta theory. Finally, systematic trends in the strength functions and level densities are examined for Sm and isotopes of neighboring elements. Some insight into these trends is obtained from the nuclear structure.

EXPERIMENTAL DESCRIPTION

The total neutron cross section of ^{151}Sm was measured by the time-of-flight method using the Rensselaer Polytechnic Institute linear electron accelerator. Transmission data were obtained over an energy range from 0.01 eV to about 2.5 keV. The standard neutron producing tungsten target and 2.5 cm thick polyethylene moderator were used for the pulsed neutron source and the flight path was 31.6 m. Neutrons were detected

TABLE I. Sm mass spectrometric sample analysis (analysis performed at Oak Ridge National Laboratory).

Isotope	Sample concentration (at.%)
^{144}Sm	< 0.001
^{147}Sm	0.937
^{148}Sm	0.041
^{149}Sm	0.166
^{150}Sm	3.09
^{151}Sm	93.11
^{152}Sm	2.39
^{153}Sm	< 0.002
^{154}Sm	0.263

with a 1.3 cm thick ^{6}Li glass scintillator mounted on an XP-1041 phototube. Two ^{151}Sm samples plus an empty sample holder and a notch filter sample were automatically cycled in and out of the neutron beam. The counting data were accumulated in 6144 time channels using an on-line computer.

The ^{151}Sm samples were 1.9 cm diam metallic disks which were prepared at the ORNL Target and Isotopes Center. The two samples weighed 204.1 and 52.0 mg and were enriched to 93.11 at.% ^{151}Sm. These weights correspond to 0.2858×10^{-3} and 0.0728×10^{-3} atom/b for the thick and thin sample, respectively. A detailed mass spectrometric analysis performed at ORNL is summarized in Table I.

Two different sets of data runs were made. The first set was designed to measure the thermal cross section and the low energy resonance region up to about 20 eV; the second provided transmission data with good resolution and counting statistics from 6 eV to above 2 keV. Experimental parameters for the two measurements are cited in Table II. Counting statistics for the resonance region ranged from less than 1% uncertainty at 450 eV and above to about 2.5% at 15 eV. Similar statistical precision obtained for the thermal energy data. The time dependent background was determined from the counting rate at saturated resonances in the notch filter sample. The steady state background was measured by adding a thick ^{10}B or cadmium filter to the notch filter sample for a few of the runs. Saturated resonances at 2.85 keV, 337 eV, 132 eV, and 18.8 eV in Na, Mn, Co, and W, respectively, were used for the resonance measurement and at 2.85 keV, 132 eV, and 1.46 eV in Na, Co, and In for the thermal measurement. The background was 5% or less of the open beam counting rate for both sets of measurements. Various sample-in, sample-out, and background runs were normalized by means of a thin foil fission chamber detector which was always in the neutron beam.

ANALYSIS OF DATA

The raw counting data for the two ^{151}Sm samples were corrected for the measured experimental background and then converted to the standard transmission function (sample in/sample out). The counting rates were sufficiently small so that dead time losses were negligible. Neutron resonances in the transmission function were analyzed by both shape and area methods, using the Atta-Harvey[5] computer codes. The shape method consists of a three parameter fit for E_0, $g\Gamma_n^0$, and Γ: the resonance energy, reduced neutron width, and total width, respectively. This is only applicable when the experimental resolution broadening and Doppler broadening are less than the natural width Γ. Thus, shape analysis could only be carried out up to 20 eV where the Doppler broadening becomes comparable to Γ.

Since the area in a resonance is to a good approximation, independent of Doppler or resolution broadening, the method of area analysis was applied to all observed resonances from thermal neutron energies up to 300 eV. This provided a verification of those reduced neutron widths determined by shape analysis. The area method uses

TABLE II. Summary of experimental parameters.

Experiment	Burst Width (ns)	Rep. rate (pps)	Time channel distribution No. × width (μs)	Samples Sm(atom/b) × 10^3	Resolution at 2 eV	20 eV	1 keV
Resonance	60	550	500×0.03125 1500×0.0625 4000×0.125 144×2.0	0.2858	•••	4.4 ns/m	2.7 ns/m
Thermal	160	30	1500×0.5 2000×1.0 2500×8.0 144×64.0	0.2858 0.0728	32 ns/m	16.6 ns/m	•••

TABLE III. Resonance parameters for $n+^{151}$Sm.

Shape and area analysis

E_0 (eV)	Γ (mV)	$g\Gamma_n^0$ (mV)	Γ_γ (mV)
0.456	100 ± 8	0.019 ± 0.001	100 ± 8
1.086	98.9 ± 2.0	0.393 ± 0.005	98.1 ± 2.0
1.697	92.6 ± 4.5	0.146 ± 0.004	92.2 ± 4.5
2.027	82.5 ± 3.9	0.223 ± 0.005	81.9 ± 4.0
4.128	94.5 ± 7.6	0.263 ± 0.010	93.4 ± 7.7
6.392	92.2 ± 6.2	1.09 ± 0.04	86.7 ± 7.0
10.33	117 ± 6.0	1.91 ± 0.08	105 ± 7
11.13	84 ± 12	0.51 ± 0.02	81 ± 12
12.67	104 ± 53	0.19 ± 0.02	103 ± 53
15.18	•••	0.108 ± 0.004	(96)
16.80	119 ± 4	1.25 ± 0.03	109 ± 5
17.33	117 ± 4	1.84 ± 0.03	102 ± 5
18.43	125 ± 13	0.92 ± 0.11	117 ± 14
18.61	119 ± 24	0.47 ± 0.11	115 ± 25
20.65	•••	0.41 ± 0.01	(96)

Area analysis only (Γ_γ = 96 mV)

E_0 (eV)	$g\Gamma_n^0$ (mV)	E_0 (eV)	$g\Gamma_n^0$ (mV)	E_0 (eV)	$g\Gamma_n^0$ (mV)	E_0 (eV)	$g\Gamma_n^0$ (mV)
21.87	0.23 ± 0.01	71.0	0.47 ± 0.04	125.9	0.33 ± 0.13	195.0	0.61 ± 0.23
22.83	0.093 ± 0.008	72.1	0.39 ± 0.05	127.7	0.97 ± 0.13	200.9	0.39 ± 0.23
25.36	0.575 ± 0.013	73.9	0.64 ± 0.05	130.3	1.55 ± 0.16	204.4	1.32 ± 0.28
28.30	0.432 ± 0.15	74.7	1.71 ± 0.06	137.5	0.87 ± 0.12	207.0	1.03 ± 0.26
30.66	0.363 ± 0.017	75.6	0.55 ± 0.06	138.3	2.38 ± 0.18	208.1	1.64 ± 0.26
32.74	0.361 ± 0.015	79.2	0.80 ± 0.07	141.1	2.40 ± 0.19	209.6	0.91 ± 0.26
34.80	0.124 ± 0.019	80.5	0.44 ± 0.05	143.6	1.35 ± 0.18	213.1	2.81 ± 0.39
36.91	0.90 ± 0.03	81.2	0.42 ± 0.06	146.2	0.08 ± 0.07	218.5	0.89 ± 0.31
37.30	0.20 ± 0.02	82.1	0.30 ± 0.05	147.9	0.52 ± 0.15	228.7	1.20 ± 0.31
38.55	0.11 ± 0.02	86.1	0.31 ± 0.06	148.8	0.37 ± 0.12	232.0	3.10 ± 0.38
39.45	0.81 ± 0.03	88.0	1.20 ± 0.07	150.5	1.60 ± 0.16	234.5	2.90 ± 0.42
41.81	1.04 ± 0.04	88.8	0.44 ± 0.07	152.1	1.29 ± 0.17	238.3	1.70 ± 0.37
44.17	0.68 ± 0.04	92.3	0.15 ± 0.06	154.6	0.56 ± 0.15	239.5	4.20 ± 0.43
47.25	0.51 ± 0.03	93.4	0.12 ± 0.06	159.5	1.11 ± 0.19	244.2	0.67 ± 0.34
48.17	0.14 ± 0.03	95.0	0.20 ± 0.07	162.4	0.84 ± 0.19	248.0	0.65 ± 0.33
49.49	0.29 ± 0.03	96.6	2.00 ± 0.10	164.3	0.81 ± 0.18	251.7	2.80 ± 0.46
50.67	1.03 ± 0.04	97.3	0.30 ± 0.07	167.3	0.50 ± 0.17	255.4	2.16 ± 0.39
54.76	0.29 ± 0.03	99.6	0.40 ± 0.07	169.8	1.61 ± 0.22	259.5	0.98 ± 0.36
56.3	0.08 ± 0.03	100.8	1.70 ± 0.11	175.6	0.98 ± 0.22	261.3	1.55 ± 0.37
57.3	0.51 ± 0.04	103.0	0.11 ± 0.08	177.6	1.30 ± 0.21	264.6	3.72 ± 0.51
58.8	2.61 ± 0.06	104.1	0.09 ± 0.07	180.8	1.22 ± 0.22	266.9	1.41 ± 0.39
59.6	0.058 ± 0.032	105.3	0.55 ± 0.09	182.3	0.52 ± 0.19	272.3	1.15 ± 0.44
60.4	0.13 ± 0.03	118.8	0.87 ± 0.12	183.2	0.69 ± 0.17	281.8	3.30 ± 0.58
66.2	0.14 ± 0.04	122.2	0.54 ± 0.12	184.3	0.94 ± 0.19	288.9	1.18 ± 0.45
66.5	0.20 ± 0.04	123.5	0.20 ± 0.10	186.3	0.76 ± 0.24	292.4	1.31 ± 0.47
68.1	0.42 ± 0.04	124.1	0.52 ± 0.12	192.5	0.40 ± 0.23	295.7	2.20 ± 0.49
70.6	0.46 ± 0.04						

the area within resonance dips in the transmission function to determine values of $g\Gamma_n^0$ for assumed values of Γ. However, for thin samples with transmission greater than ~70%, the reduced neutron width is essentially independent of Γ. This situation obtained for nearly all of the resonances observed above 20 eV. Resonances in the thin Sm sample were too small to be analyzed above 14 eV as this sample was primarily designed for the thermal cross section measurement.

Thick and thin sample data for the ^{151}Sm cross section from 0.01–2.5 eV were averaged and then analyzed separately after all the resolved resonance parameters had been determined. The two

samples yielded the same cross section within statistical uncertainties. A small (4.4% max) correction was applied to account for 0.166 at.% ^{149}Sm present in the samples. The cross section calculated from the resolved resonance parameters was subtracted from the observed cross section and the remaining cross section was fitted by trial and error to determine the parameters of the bound states. Only one bound state resonance was needed to fit the data.

The average cross section in the keV range was also determined from the transmission data, as were the resonance spacing and the strength function. These aspects of the analysis are discussed separately later.

RESULTS

A. Resonance parameters and epithermal cross section

The transmission data were analyzed up to about 300 eV and resonance parameters were determined. Above this energy the transmission dips have become too small for reliable analysis due to the decreased resonance amplitude and the increasing Doppler and resolution broadening. Up to 105 eV it is reasonably certain that no resonances were missed, at higher energies the fraction of missed resonances increases throughout the analyzed region. Between 200 and 300 eV more than half of the individual resonances were not resolved. In many cases the fitted fluctuations in the transmission function contain two or more resonances. However, the derived resonance parameters do provide a satisfactory fit to the data and the strength function is constant within statistics for the entire energy range. The resonance parameters are listed in Table III and Figs. 1–3 compare the experimental transmission function with that calculated from the resonance parameters.

Radiation widths Γ_γ were obtained for 13 resonances. The error weighted average value of 96 mV is somewhat higher than one might expect for a typical rare earth isotope, but this is probably due to the very high level density near the midpoint of filling the $1h_{9/2}$-$2f_{7/2}$ shells. In general agreement with this result, radiation widths determined by Rahn *et al.*[6] for ^{151}Eu and ^{153}Eu were 90.0 and 94.8 mV, respectively. The ^{151}Sm radiation widths were constant within 10% of the average value for most resonances and within 20% for all but one resonance.

The neutron capture resonance integral RI $= \int_{0.5\text{eV}}^{\infty} \sigma_{n\gamma}(E)/E\,dE$ was computed from the resolved resonance parameters by explicit numerical integration of the cross section. The average ra-

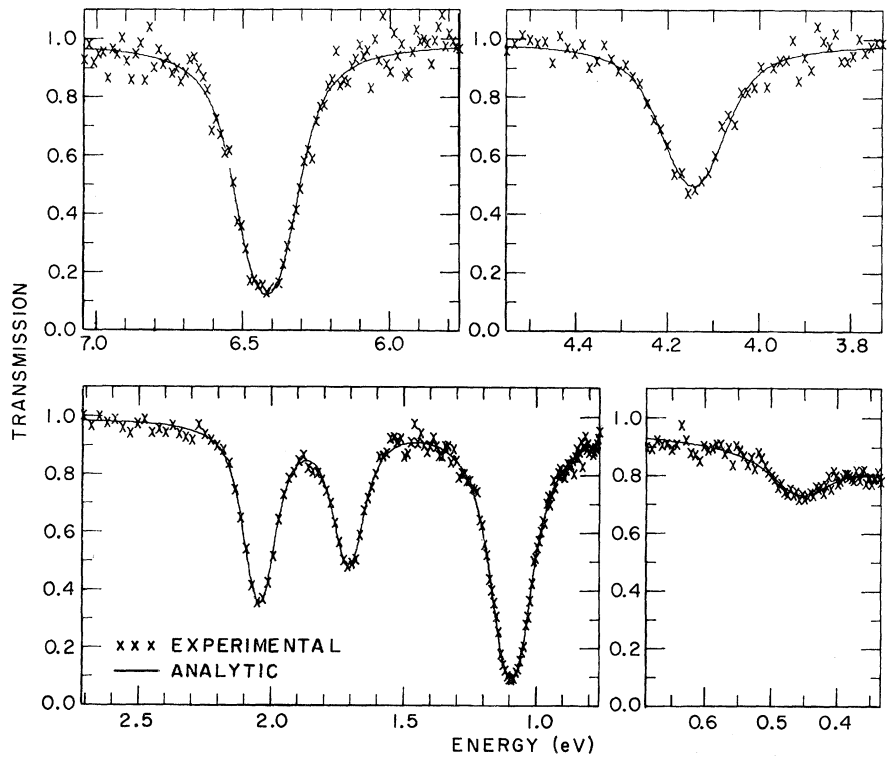

FIG. 1. Transmission data and calculated resonance cross section for ^{151}Sm below 10 eV.

diation width was used where individual values were unavailable. The resonance integral was determined to be 3520 ± 160 b in good agreement with Pattenden's[3] value of 3300 ± 700 b. Our result includes a contribution of 170 b for the unresolved resonances above 300 eV. About 73% of the resonance integral comes from resonances below 12 eV with the 1.09 eV resonance alone contributing 39%. Although the bound state resonance essentially makes up the entire thermal energy cross section, it contributes only 91 b to the resonance integral above 0.5 eV.

The resonance parameters in Table III have been compared with Pattenden's[3] 1963 results. Since his samples were prepared from fission product Sm containing less than 4% of ^{151}Sm, the resonance dips in transmission are much smaller and more difficult to analyze than in the present measurements. In hindsight, considering the difficulty of working with low enrichment fission product Sm, his results were very accurate. Several general comments are in order:

(1) The ^{151}Sm resonance at 0.46 eV was not observed by Pattenden due mostly to the statistical scatter of the points; however, a hint of its presence is there.

(2) The resonance at 5.33 eV which he attributes to ^{151}Sm is definitely due to a large resonance in ^{147}Pm. Extensive resonance data are now available for ^{147}Pm[7,8] and they confirm this assignment as well as explain the large resonances observed by Pattenden at 40.8, 48.3, and 65.5 eV.

(3) The resonance doublet reported by Pattenden at 4.09 and 4.19 eV was accurately described in our data by a single resonance at 4.13 eV. The sum of his two reduced neutron widths agrees with our single reduced width within 5%.

(4) The neutron widths reported here for the resonances at 1.09, 1.70, and 2.03 eV are some 15 to 25% larger than those previously reported. All other resonance parameters agree within the quoted uncertainty.

B. Thermal energy cross section

The measured ^{151}Sm total cross section at thermal neutron energies is shown in Fig. 4. A correction for the ^{149}Sm present in the samples has been applied. This correction reaches 4.4% at 0.87 eV, the ^{149}Sm resonance energy, but is essentially negligible away from the resonance. The cross section at 0.0253 eV is 15 200 b in good agreement with the value of 15 000 b previously reported by Pattenden.[3]

The effect of nearby bound states is extremely important in ^{151}Sm. The resolved resonances contribute only 1.7% to the total cross section at 0.0253 eV. This portion of the cross section was subtracted from the measured total and the remaining part was fitted by trial and error to de-

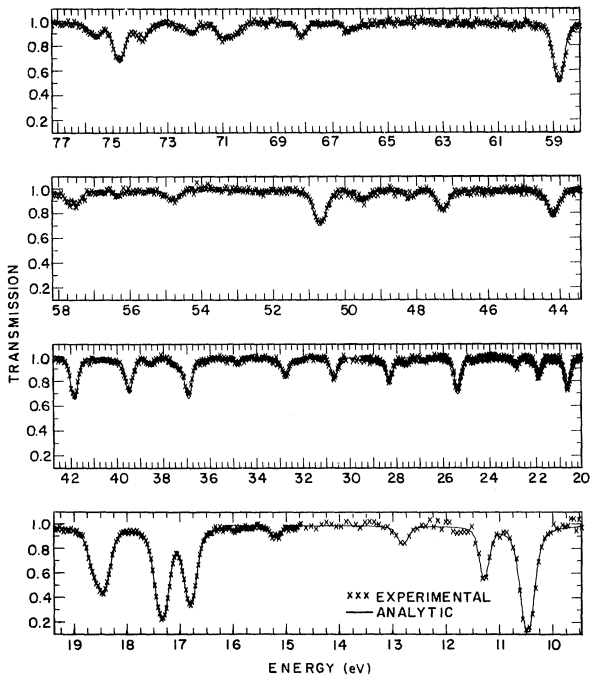

FIG. 2. Fitted transmission data for ^{151}Sm between 10 and 78 eV.

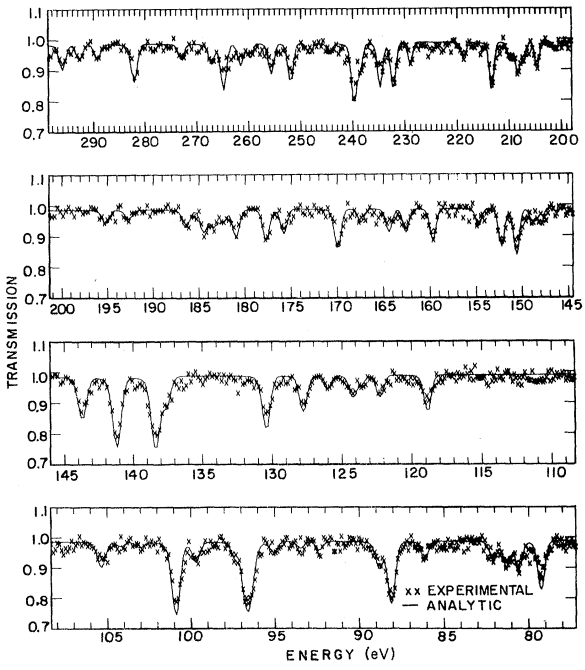

FIG. 3. Fitted transmission data for ^{151}Sm above 78 eV.

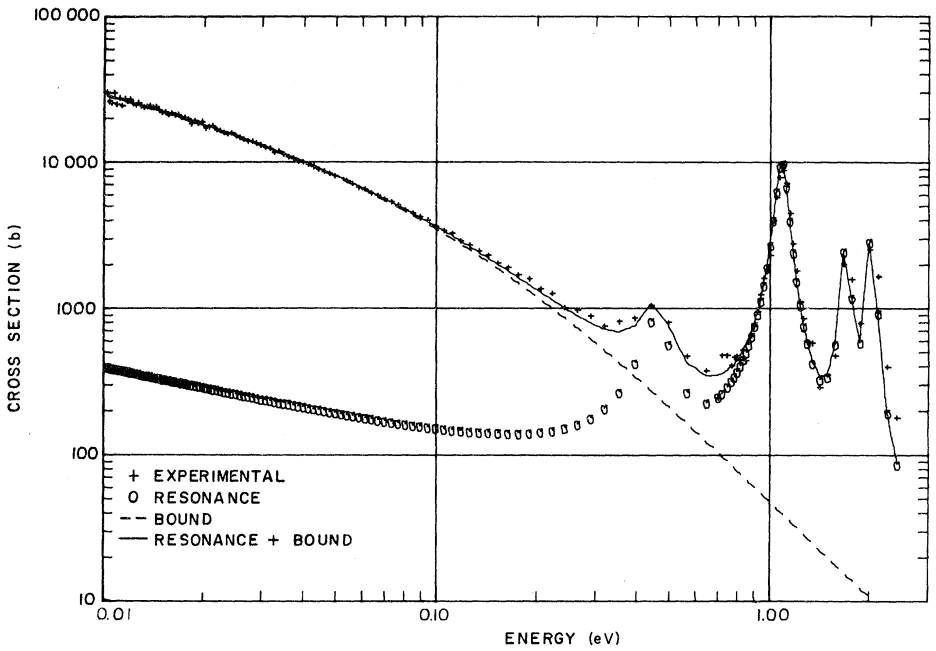

FIG. 4. The energy dependent thermal cross section of ^{151}Sm. The solid line shows the fitted cross section as computed from the resolved and bound resonance parameters. The bound state and resonance components are also shown separately.

termine the resonance parameters of bound states. A good fit, accurate within the statistical uncertainty of the measurement, was achieved by using a single state at −0.12 eV. The state also has sensible resonance parameters, 100 mV for Γ_γ and 0.848 mV for $g\Gamma_n^0$. Figure 4 shows the bound and resolved components of the cross section. The ^{151}Sm cross section is strongly non-$1/v$ even at 0.025 eV and use of a 15 000 b $1/v$ cross section would overestimate the thermal neutron capture rate.

C. Cross section in the low keV energy range

In the 300–2250 eV energy range the measured transmission function was used to determine the average cross section. Although the transmission is typically greater than 90% in this energy range, the statistical precision in each time channel is better than 2% and thus the computation of an average cross section seemed justified.

One difficulty inherent in the determination of the average cross section from high transmission samples is the evaluation and elimination of any systematic base-line bias due to small normalization errors between sample-in and sample-out runs. However, this bias can be determined by fitting the average cross section to a function of the form $A+B/\sqrt{E}$. The constant A contains the unknown bias and the potential scattering cross section. The coefficient B is directly related to the strength function. Higher order terms do arise in this expansion,[9] but they were negligible for ^{151}Sm in the lower keV energy range. The constant A was found to be 39 b which includes an assumed 8 b of potential scattering. The strength function determined as above was in excellent agreement with that derived from individual resonance parameters.

The average cross section with bias and potential scattering removed, is shown in Fig. 5 for 25, 51, and 101 point averages. These averages correspond to energy averaging intervals of approximately 50, 100, and 200 eV at 1 keV. The residual "intermediate structure" which can be seen in the cross section is quite interesting. The fluctuation near 800 eV for example contains about 75 compound nucleus resonances.

D. Level density and the Dyson-Mehta Δ statistic

The level density of ^{152}Sm just above the neutron separation energy (~8.30 MeV) was determined from the observed spacing of resonances in the $n+^{151}$Sm total cross section for neutron energies 0–105 eV. This region includes 64 resolved resonances. The level density was obtained by least squares fitting the cumulative density of states $N(E)$, the usual stair step function, to a straight line function AE_n+B. The values obtained for the

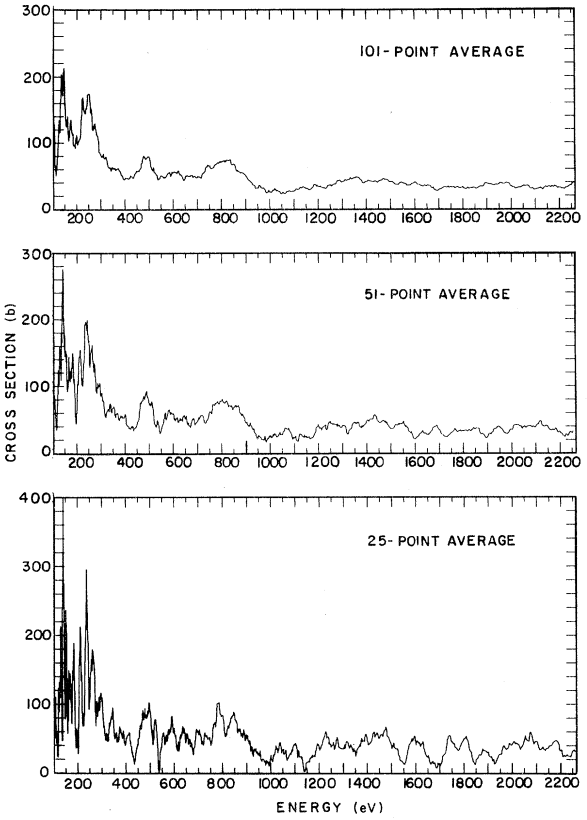

FIG. 5. The average total cross section for ^{151}Sm from 100 to 2250 eV. The potential (hard sphere) scattering cross section has been subtracted. The three averaging intervals correspond to approximately 50, 100, and 200 eV.

zero offset level spacing $1/B$ and the average level spacing $1/A$ were 0.607 and 1.722 eV, respectively. The average level spacing value of 1.722 eV corresponds to a ^{152}Sm level density of 5.807×10^5 states/MeV at 8.30 MeV.

The above fitting is a necessary preliminary step for the computation of the Dyson-Mehta[10] (D-M)Δ_3 statistic. This statistic is defined as,

$$\Delta_3 = \underset{A,B}{\mathrm{Min}} \frac{1}{E_{\max}} \int_0^{E_{\max}} [N(E) - AE - B]^2 dE .$$

Theoretical values for Δ_3 have been derived by Dyson and Mehta based on the statistical orthogonal ensemble[11] (OE). This theory for the statistical properties of the eigenvalues of large random matrices implies a long range ordering of level spacings such that Δ_3 increases only as $\ln N$ rather than proportional to N, which follows from a purely random sequence of spacings (no long range order). Rahn *et al.*[6] and Camarda *et al.*[12] have recently tested the Δ_3 statistic on a sequence of levels observed in ^{152}Sm, ^{154}Sm, and several other rare earth neutron cross sections. Good agreement between theory and observation was obtained. The Δ_3 statistic has not yet been tested on level sequences in the odd A isotopes of Sm nor for ^{150}Sm. Since extensive resonance data now exist for ^{147}Sm and ^{150}Sm (Eiland *et al.*[13]), for ^{149}Sm (Karzhavina and Popov[14]), and for ^{151}Sm, it is of interest to compute the Δ_3 statistic for these isotopes also.

Table IV lists these results for six Sm isotopes. The Δ_3 statistic for ^{152}Sm and ^{154}Sm were included in the table. For these two isotopes, we used the same level sequences as did Rahn *et al.*[6] in order to verify our calculations. Our results are identical to theirs. The second and third columns of the table indicate the number of levels in each sequence and the upper energy limit. The upper energy limit for each isotope, $E_{\max}$, was selected by examing the plot of $N(E)$ vs E. Since it is required that the level sequence be complete up to $E_{\max}$, this limit was conservatively chosen. Figure 6 shows the function $N(E)$ vs E for ^{151}Sm and indicates the selection of $E_{\max}=105$ eV. The theoretical values of Δ_3 and their standard deviations were computed in accordance with Eqs. (81) and (82), D-M Ref. 10, for the odd A isotopes and Eqs. (58) and (64) for the even A isotopes.

Table IV shows that the level sequences for all six Sm isotopes have the long range order predicted by the D-M theory. Thus the present new results for ^{147,149,150,151}Sm provide further confirmation of the theory. A reasonable alternative to the D-M theory is the usual (uncorrelated) Wig-

TABLE IV. Summary of results for the Dyson-Mehta Δ_3 statistic.

Target isotope	N_{tot}	$E_{\max}$ (eV)	Δ_3 Observed	Δ_3 D-M theory	Δ_3 U-W theory	$\bar{D}$ (eV)	Ref.
^{147}Sm	43	291.4	0.70	0.61 ± 0.22	0.92 ± 0.49	7.00	13
^{149}Sm	53	127.1	0.51	0.65 ± 0.22	1.10 ± 0.60	2.38	14
^{150}Sm	11	556.0	0.15	0.24 ± 0.11	0.31 ± 0.13	56.5	13
^{151}Sm	64	105.2	0.54	0.69 ± 0.22	1.30 ± 0.73	1.72	
^{152}Sm	70	3365.0	0.40	0.42 ± 0.11	1.35 ± 0.81	53.8	6
^{154}Sm	27	3046.8	0.37	0.32 ± 0.11	0.57 ± 0.31	112.6	6

ner (U-W) distribution of level spacings. Using Monte Carlo techniques, Camarda *et al.*[12] have derived expressions for Δ_3 from the U-W distribution. This result is given in column 6 of the table. It can be seen that the observed Δ_3 statistic is in much better agreement with the D-M theory than the U-W result. However, the standard deviations of the U-W result are somewhat too large due to the limited population of s-wave resonances to be absolutely conclusive.

Previous to the present results and recent work by the Columbia group[6,12,22] and by Coceva *et al.*,[23] all computed values of Δ_3 were much larger than $\Delta_{D\text{-}M}$. It was generally assumed that this was due to errors in the experimental level sequence due to missed weak s-wave resonances or to erroneous inclusion of p-wave resonances. This assumption was indeed borne out in our analysis for ^{147}Sm. Our initial selections for N and E_{max} for this isotope were 81 and 600 eV, respectively, because the stair step plot *appeared* to be a straight line up to that energy. The selection leads to an observed Δ_3 of 1.22 compared to $\Delta_{D\text{-}M}$ of 0.74 ± 0.22. When N and E_{max} were very conservatively lowered to 43 and 291.4 eV, the result in Table IV was obtained, in good agreement with $\Delta_{D\text{-}M}$.

E. Strength function

The neutron strength function for the $n + ^{151}$Sm interaction was determined by two different methods: (1) from the low energy resolved resonances and (2) from the average cross section in the keV energy range. Up to 296 eV, 120 resonances have been analyzed in the ^{151}Sm neutron total cross section. Due to the low p-wave penetrability at these energies and the near minimum p-wave strength function in this mass region, it can be confidently asserted that all of these resonances are s wave. However, due to the nonzero ground state spin for ^{151}Sm ($I = \frac{5}{2}^-$) s-wave resonances form a dual population with total angular momentum, $J = I \pm \frac{1}{2}$, of either 2^- or 3^-. Since resonances with $J = 2^-$ or 3^- cannot be distinguished by analysis of the total cross section, only the total s-wave strength function averaged over both spin states can be determined.

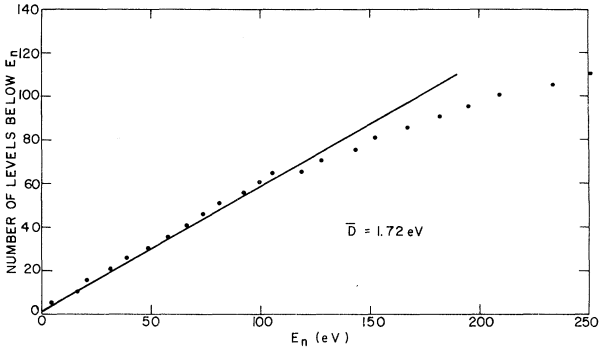

FIG. 6. Average level spacing of s-wave neutron resonances in $n + ^{151}$Sm. The points are plotted at intervals of five resonances. Note the appreciable number of unresolved resonances above 110 eV.

The s-wave strength function S_0 was obtained from the cumulative sum $\sum g\Gamma_n^0$ for resolved resonances, divided by the width of the analyzed energy region (i.e., $S_0 = \sum g\Gamma_n^0 / \Delta E$). It is frequently stated that this method is insensitive to missed resonances because the missed resonances have small $g\Gamma_n^0$ values and contribute little to the cumulative sum. For ^{151}Sm it can be seen from Fig. 6 that some resonances probably begin to be undetectable above 110 eV. The insensitivity of the strength function to weak missing resonances is demonstrated in Table V where the S_0 derived from three 100 eV analysis subintervals is shown. Although the apparent level density drops by more than a factor of 2 from 100 to 300 eV, the strength function is constant within its statistical uncertainty. Indeed, the apparent increase in strength between 200–300 eV appears to be a real statistical or intermediate structure fluctuation (see Fig. 5). The same information given in Table V is graphically illustrated in Fig. 7 which shows the function $\sum g\Gamma_n^0$ vs E. Although the plot of the cumulative number of levels (Fig. 6) begins to bend above 110 eV, the strength function remains nearly constant. The straight line in Fig. 7 represents the best value of the strength function $S_0 = 3.23 \pm 0.47$, de-

TABLE V. s-wave strength function for ^{151}Sm.

Energy range (eV)	N Local levels	N_c Cumulative	$S_0 \times 10^4$ Local	$S_0 \times 10^4$ Cumulative
0–100	60	60	3.34 ± 0.61	3.34 ± 0.61
100–200	35	95	3.11 ± 0.74	3.23 ± 0.47
200–296	25	120	4.71 ± 1.33	3.71 ± 0.48
100–2270	(energy averaged cross section)			3.59

Best over-all value: $S_0 = 3.65 \pm 0.48 \times 10^{-4}$

termined from the resolved resonances below 200 eV.

A second independent determination of the s-wave strength function was obtained from the measured cross section in the low keV energy range. A 101 point average (approximately 200 eV averaging interval) of the cross section was performed in the energy range from 100–2270 eV. This result was previously shown in Fig. 5. The averaged cross section was then fitted to a function of the form $A+B/\sqrt{E_n}$. This result was originally derived by Feshbach, Porter, and Weisskopf[15] from the optical model and was written in terms of the strength function as,

$$\bar{\sigma}_{\text{total}} = \frac{2\pi^2 \lambda\!\!\!^{-}_1{}^2}{\sqrt{E}} S_0 + 4\pi R'^2 ,$$

where $\lambda\!\!\!^{-}_1$ is the wavelength of a 1 eV neutron and R'^2 is the potential scattering length. More accurate forms of this equation have since been derived[9] for the higher keV energy range, but for the present purpose R' can be considered a constant and the higher order term in $S_0{}^2$ is negligible. The strength function derived from fitting the average cross section was $S_0 = 3.59\times10^{-4}$, in good agreement with that derived from the lower energy resolved resonances. Averaging these two determinations of S_0, we obtain $S_0 = 3.65 \pm .48\times10^{-4}$ for the best over-all value for ^{151}Sm.

SYSTEMATICS OF Sm LEVEL DENSITIES AND STRENGTH FUNCTIONS

The agreement of known level sequences in the Sm isotopes with the Dyson-Mehta theory indicates that these sequences are complete. Thus, the level spacings provide a reliable measure of the $l=0$ compound nucleus level density at an excitation energy equal to the neutron binding energy. The mass region spanned by the Sm isotopes begins with a major, $N=82$, shell closure at ^{144}Sm and extends well up into the filling of the $2f_{7/2}$ and $1h_{9/2}$ shells. It is therefore of interest to examine the systematic behavior of the level density vs neutron number.

In order to eliminate the influence of pairing and excitation energy on the level density, the Fermi level density parameter a (MeV^{-1}) was derived from the experimentally determined level density. The Bethe formula, as given by Gilbert and Cameron,[16] was used:

$$\rho(U) = \sum_{J(l=0)} \frac{\pi^{1/2}}{12} \frac{\exp[2(aU)^{1/2}]}{a^{1/4}U^{5/4}} \times \frac{(2J+1)\exp[-(J+\frac{1}{2})^2/2\sigma^2]}{2(2\pi)^{1/2}\sigma^3} ,$$

where $U = B_n - \delta_n - \delta_p$ (MeV) is the compound nucleus excitation energy with pairing energy corrections; J is the compound nucleus total angular momentum, $\sigma^2 = 0.0888\sqrt{Ua}\,A^{2/3}$ is the spin-cutoff factor, and a is the derived level density parameter (MeV^{-1}). The pairing energies determined by Cameron and Elkin[17] from a semiempirical mass formula were used. Although the spin-cutoff factor should be treated as a second free parameter, we have used the above shell model estimate based on the neutron and proton single-particle level spacings. This procedure seems justified since σ is nearly constant and the level density is much less sensitive to σ than to a.

The results derived for the density parameter

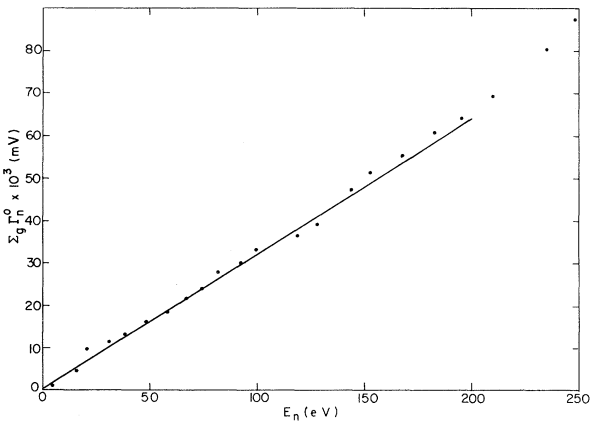

FIG. 7. The s-wave neutron strength function for ^{151}Sm as derived from $\Sigma g\Gamma_n^0$ vs E. Points are shown at intervals of five resolved resonances. The linearity of $\Sigma g\Gamma_n^0$ vs E, in spite of the large number of missed resonances above 110 eV, is noteworthy.

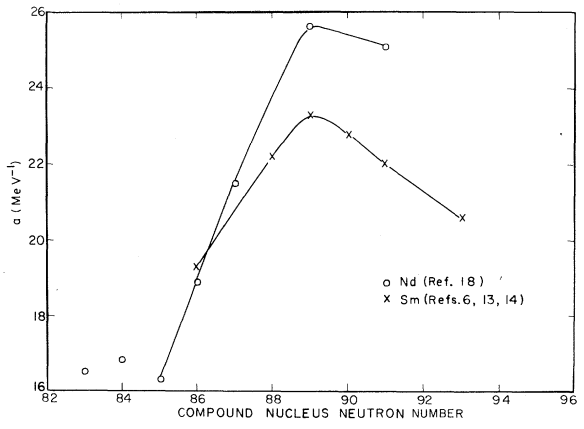

FIG. 8. The Fermi level density parameter a (MeV^{-1}) vs the compound nucleus neutron number for Sm and Nd isotopes. The low values for N approaching 82 are explained by shell closure, while the decreasing values above $N=89$ appear to be associated with increasing nuclear deformation (see text).

TABLE VI. Level density parameters for Sm and Nd isotopes.

Target Nucl.	Compound nucl. Z	N	B_n (MeV)	δ_p (MeV)	δ_n (MeV)	σ	$\rho_0 \times 10^{-5}$ (MeV^{-1})	a (MeV^{-1})
^{147}Sm	62	86	8.144	−1.22	−0.92	5.17	1.43	19.3
^{149}Sm	62	88	7.986	−1.22	−0.99	5.33	4.20	22.2
^{150}Sm	62	89	5.596	−1.22	•••	5.04	0.177	23.3
^{151}Sm	62	90	8.258	−1.22	−1.10	5.42	5.81	22.8
^{152}Sm	62	91	5.870	−1.22	•••	5.10	0.186	22.0
^{154}Sm	62	93	5.814	−1.22	•••	5.00	0.0888	20.6
^{142}Nd	60	83	6.070	−1.18	•••	4.67	0.0241	16.5
^{143}Nd	60	84	7.814	−1.18	0.76	4.92	0.313	16.8
^{144}Nd	60	85	5.970	−1.18	•••	4.65	0.0186	16.3
^{145}Nd	60	86	7.580	−1.18	0.92	5.00	0.529	18.9
^{146}Nd	60	87	5.150	−1.18	•••	4.77	0.0474	21.5
^{148}Nd	60	89	4.950	−1.18	•••	4.94	0.1389	25.6
^{150}Nd	60	91	4.800	−1.18	•••	4.90	0.0826	25.1

a by the above procedure are listed in Table VI along with the other relevant parameters. The relationship between a and the neutron number is graphically illustrated in Fig. 8. The level density parameter demonstrates a well defined maximum at $N=89$ ($A=151$ for Sm). A similar trend was observed by Karzhavina *et al.*[18] for seven isotopes of Nd. Since they used a different compilation of pairing energies, it was decided to repeat their calculation using the same pairing energies as for Sm and with the more recent Nd data of Tellier and Newstead.[19] The trend was essentially the same as seen by Karzhavina *et al.* This result is also shown in Fig. 8 and Table VI. The behavior of a vs N for the Nd isotopes appears to be in full agreement with that for the Sm isotopes.

The small values for the level density parameter for neutron numbers approaching $N=82$ seems clearly explained by the shell closure at this magic number. However, the decreasing values of a above $N=89$ are not so easily explained by shell model arguments. The increase between $N=82$ and 89 may be correlated with the number of valence particles or holes in the $f_{7/2}$ and $h_{9/2}$ shells. The tendency for the level density to maximize at the half filled shell and to decrease for fewer particles or holes is predicted in the work of Rosenzweig.[20] Between $N=82$ and 89 the Sm and Nd isotopes are spherical, or nearly so, and the $f_{7/2}$ and $h_{9/2}$ shells are very close to each other in energy, nearly degenerate. If these shells are treated as a single "super shell" holding 18 particles, then the level density should maximize at $N=91$. However, beginning around $N=88$ or 89, the target nuclei, for example ^{149}Sm or ^{150}Sm begin to be appreciably deformed. In this case the Nilsson[21] level sequence must be followed rather than that for a spherical potential. If we examine the Nilsson diagram for $82 \leq N \leq 126$, there is a definite energy gap at $N=90$ for values of deformation, $\delta \sim 0.26$, which are characteristic of ^{152,154}Sm. This gap simulates the effect of a shell closure and should therefore lead to a decreased density. It is possible that this effect, which arises for deformed nuclei, is the cause of decreased values of a above $N=89$.

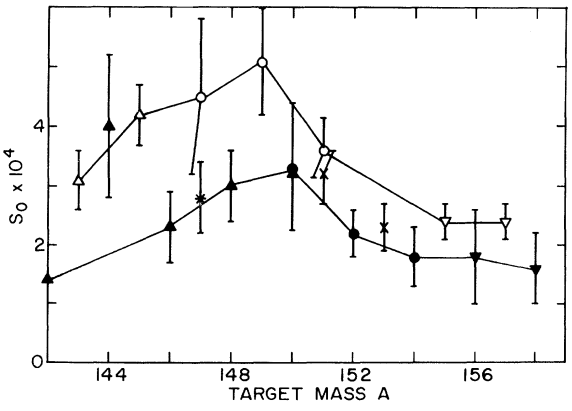

FIG. 9. The s-wave neutron strength function for Sm and neighboring isotopes in the region of the first peak of the 4-s giant resonance. The curves are intended merely as guides to the eye to illustrate the difference between odd and even neutron targets.

The strength functions for the Sm isotopes and for neighboring isotopes are illustrated in Fig. 9. These data demonstrate a strong even-odd fluctuation of the strength function in this mass region. If smooth curves are drawn through the even-even and even-odd strength functions, as shown, it becomes clear that the even-odd target strength functions are systematically larger by nearly a factor of 2 in the peak region. The one deviation from this trend is the strength function for ^{144}Nd, but here the uncertainty of the value is large.

These odd-even fluctuations suggest some influence due to pairing correlations and merit further investigation.

We thank Barbara L. Hennig for her competent work in the storage, retrieval, and transformation of data and for the construction of a multitude of computer graphs. The efforts of Leon Love of the Target and Isotopes Division at Oak Ridge National Laboratory is gratefully acknowledged for the separation and production of the metallic ^{151}Sm samples.

---

*Operated for the U.S. Atomic Energy Commission by the General Electric Company under Contract No. W-31-109-Eng-52.

[1]F. E. Lane and W. H. Walker, in Proceedings of the Second Conference on Neutron Cross Sections and Technology, Washington, D.C., March 1968, edited by D. T. Goldman (NBS Special Publication No. 299, 1968), Vol. I, p. 381.

[2]R. J. French, in Proceedings of the Second Conference on Neutron Cross Sections and Technology, Washington, D.C., March 1968 (see Ref. 1), p. 259.

[3]N. J. Pattenden, Nucl. Sci. Eng. 17, 371 (1963).

[4]W. H. Walker, Chalk River Laboratory Report No. AECL-3037, 1973 (unpublished), Pt. II.

[5]S. E. Atta and J. A. Harvey, Oak Ridge National Laboratory Report No. ORNL-3205, 1962 (unpublished).

[6]F. Rahn *et al.*, Phys. Rev. C 6, 251 (1972).

[7]J. W. Codding, Jr., R. L. Tromp, and F. B. Simpson, Nucl. Sci. Eng. 43, 58 (1971).

[8]G. J. Kirouac *et al.*, Nucl. Sci. Eng. 52, 310 (1973).

[9]K. K. Seth *et al.*, Phys. Rev. 110, 692 (1958).

[10]F. J. Dyson and M. L. Mehta, J. Math. Phys. 4, 701 (1963).

[11]F. J. Dyson, J. Math. Phys. 3, 140, 157, 166 (1962).

[12]H. Camarda *et al.*, in *Statistical Properties of Nuclei*, edited by J. B. Garg (Plenum, New York 1972), p. 205.

[13]H. M. Eiland *et al.*, Nucl. Sci. Eng. 54, 286 (1974).

[14]E. N. Karzhavina and A. B. Popov, Joint Institute for Nuclear Research Report No. JINR-P3-5655, 1971 (unpublished).

[15]H. Feshbach, C. Porter, and V. F. Weisskopf, Phys. Rev. 96, 448 (1954).

[16]A. Gilbert and A. G. W. Cameron, Can. J. Phys. 43, 1446 (1965).

[17]A. G. W. Cameron and R. M. Elkin, Can. J. Phys. 43, 1288 (1965).

[18]E. N. Karzhavina *et al.*, Yad. Fiz. 8, 639 (1968) [transl.: Sov. J. Nucl. Phys. 8, 371 (1969)].

[19]H. Tellier and C. M. Newstead, in Proceedings of the Third Conference on Neutron Cross Sections and Technology, Knoxville, Tennessee, 1971 (unpublished), Vol. II, p. 680.

[20]N. Rosenzweig, Phys. Rev. 105, 950 (1957); 108, 817 (1957).

[21]S. G. Nilsson, K. Dan. Vidensk. Selsk. Mat.—Fys. Medd. 29, No. 16 (1955); also B. R. Mottleson and S. G. Nilsson, K. Dan. Vidensk. Selsk. Mat.—Fys. Skr. 1, No. 8 (1959).

[22]H. I. Liou *et al.*, Phys. Rev. C 5, 974 (1972).

[23]C. Coceva *et al.*, in *Statistical Properties of Nuclei* (see Ref. 12), p. 447.